Nuclear mass number dependence of inclusive production of ω and φ mesons in 12 GeV p + A collisions

T. Tabaru,[*] H. En'yo, R. Muto, M. Naruki, and S. Yokkaichi
RIKEN, 2-1 Hirosawa, Wako, Saitama 351-0198, Japan

J. Chiba,[†] M. Ieiri, O. Sasaki, M. Sekimoto, and K. H. Tanaka
Institute of Particle and Nuclear Studies, KEK, 1-1 Oho, Tsukuba, Ibaraki 305-0801, Japan

H. Funahashi, Y. Fukao, M. Kitaguchi, M. Ishino,[‡] H. Kanda,[§] S. Mihara,[‡] T. Miyashita, K. Miwa, T. Murakami,
T. Nakura, F. Sakuma, M. Togawa, S. Yamada, and Y. Yoshimura
Department of Physics, Kyoto University, Kitashirakawa, Sakyo-ku, Kyoto 606-8502, Japan

H. Hamagaki and K. Ozawa
Center for Nuclear Study, Graduate School of Science, University of Tokyo, 7-3-1 Hongo, Tokyo 113-0033, Japan

The inclusive production of ω and φ mesons is studied in the backward region of the interaction of 12 GeV protons with polyethylene, carbon, and copper targets. The mesons are measured in e^+e^- decay channels. The production cross sections of the mesons are presented as functions of rapidity y and transverse momentum p_T. The nuclear mass number dependences (A dependences) are found to be $A^{0.710\pm0.021(\text{stat})\pm0.037(\text{syst})}$ for ω mesons and $A^{0.937\pm0.049(\text{stat})\pm0.018(\text{syst})}$ for φ mesons in the region of $0.9 < y < 1.7$ and $p_T < 0.75$ GeV/c.

PACS number(s): 14.40.Cs, 13.85.Ni, 13.85.Qk, 25.40.Ve

I. INTRODUCTION

The modification of the vector meson spectral function in hot and/or dense matter is currently a hot subject in terms of spontaneous chiral symmetry breaking and partial restoration of the symmetry in nuclear matter. Currently it is the focus of several experiments [1–4]. The experiment KEK-PS E325 was performed to measure the vector meson spectral functions in dense matter, i.e., the nucleus. Thus far we have reported the signature of the mass modification of vector mesons [5–7]. These observations are fairly remarkable; hence, we also performed analyses to determine the absolute cross sections and nuclear mass number dependences of the production of these mesons in order to understand the underlying production mechanism.

The nuclear mass number dependence of the cross sections for the particle production is usually parametrized as

$$\sigma(A) = \sigma_0 A^\alpha \qquad (1)$$

for a target nucleus with mass number A. When the collision energy $\sqrt{s_{NN}}$ is sufficiently large, the parameter α in the production of light mesons such as pions or ρ mesons is about 2/3 [8,9]. This can be interpreted by considering such

productions to be dominated by primary collisions at the front surface of a target nucleus. Note that the mean free path of incident protons in a nucleus is as small as 1.4 fm. On the other hand, α tends to unity in the case of hard reactions such as the production of J/ψ at high energies, $\sqrt{s_{NN}} \gtrsim 20$ GeV [9–11].

The present experiment was performed at $\sqrt{s_{NN}} = 5.1$ GeV. At higher energies, α for φ meson production was reported to be 0.81 ± 0.06, 0.96 ± 0.04, and 0.86 ± 0.02 at $\sqrt{s_{NN}} = 11.6$ [12], 14.2 [13], and 15.1 GeV [14], respectively. However, there is no reason to believe that these values are applicable at our energy. A few heavy-ion-induced experiments at $\sqrt{s_{NN}}$ from 4.9 to 5.4 GeV [15,16] reported φ meson production data, to which the present experiment can provide complementary data. Note that there have been no measurements of ω mesons and φ mesons with $p + A$ reactions at $\sqrt{s_{NN}}$ around 5 GeV.

A φ meson is almost a pure $s\bar{s}$ state. Therefore, the production of a φ meson without other accompanying strange particles is suppressed by the Okubo-Zweig-Iizuka rule [17]. This results in the effective threshold energy's being as high as $\sqrt{s_{NN}} = 3.9$ GeV, which corresponds to $2m_p + 2m_{s\bar{s}}$, since two $s\bar{s}$ pairs are effectively needed to realize the φ production. Our collision energy is fairly close to this effective threshold. In addition, the importance of additional mechanisms for φ meson production, such as an intrinsic $s\bar{s}$ component in nucleons [18] and $\phi\rho\pi$ coupling [19,20], have been suggested by theorists; however, they have thus far been insufficiently studied at our energy from an experimental viewpoint. Thus, to understand the production mechanism at our energy, basic measurements such as production cross sections and α parameters are indispensable.

————
[*]Electronic address: tsugu@riken.jp

[†]Present address: Department of Physics, Faculty of Science, Technology, Tokyo University of Science, 2641 Yamazaki, Noda, Chiba 378-8510, Japan.

[‡]Present address: ICEPP, University of Tokyo, 7-3-1 Hongo, Tokyo 113-0033, Japan.

[§]Present address: Physics Department, Graduate School of Science, Tohoku University, Sendai 980-8578, Japan.

In this article we present inclusive production cross sections and α parameters of ω and ϕ mesons measured via the e^+e^- decay channels in 12 GeV $p + p$, $p + C$, and $p + Cu$ collisions. The results are compared with those from the nuclear cascade simulation JAM [21], and the implications for production mechanisms are discussed.

II. EXPERIMENT

The spectrometer was built in the EP1-B beamline at the 12 GeV proton synchrotron in KEK. The beamline was designed to deliver a 12 GeV primary proton beam with an intensity of up to 4×10^9 protons per spill. The beam was extracted for 1.8 s with a repetition rate of 1/4 Hz. The beam intensity was monitored with about 10% accuracy by using ionization chambers [22] located downstream of the spectrometer.

Figures 1 and 2 show a top view and a side view of the experimental setup, respectively. The spectrometer was designed to simultaneously measure e^+e^- and K^+K^- pairs. A dipole magnet and tracking devices were commonly used together with electron and kaon identification counters.

The magnet was operated at 0.71 T at the center of the dipole gap and provided 0.81 T m of field integral for tracking. The magnetic field map was calculated by the finite-element-analysis software TOSCA [23]. The calculated map agreed well with the measured map, and the difference was negligible when compared with the momentum resolution of this spectrometer. During the data collection periods, the field strength was monitored every 4 s with a nuclear-magnetic-resonance (NMR) probe located at the center of the surface of the lower pole piece. The magnetic field map was scaled run by run according to the NMR data. The fluctuation of the magnetic field was found to be less than 10^{-5} within a typical run of 2 h long.
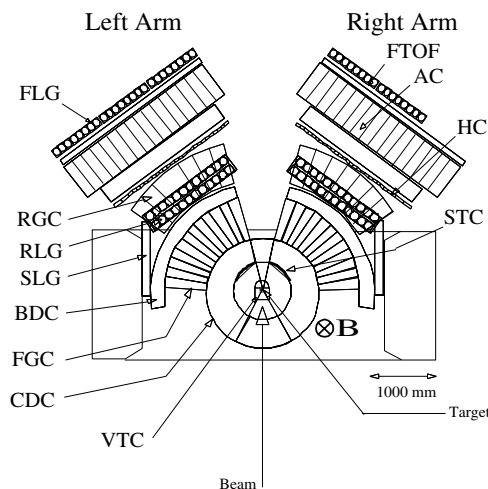

FIG. 1. Schematic view of the experimental setup from the top, which is designed symmetrically with respect to the beam. The components of this setup are referred to as left and right arms in this article.
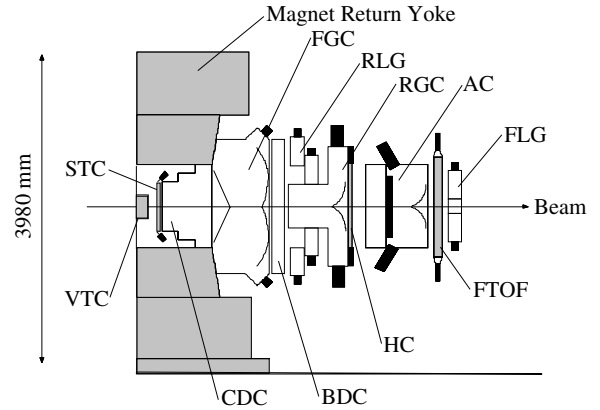

FIG. 2. Cross section of the experimental setup along the plane of the center of the kaon identification counters.

The targets were aligned inline along the beam axis at the center of the magnet. The target materials and configurations are shown in Table I.

The beam profile in the horizontal direction was measured by counting the interaction rate by changing the beam position at the target. The beam position was moved by the bending magnet located about 10 m upstream of the target. In this measurement the center target, whose thickness was 1 mm, was rotated by 90° around the vertical axis and was used as a 1 mm wide probe. The typical beam size in the horizontal direction was found to be 2.0 mm in full width at half-maximum. The beam size in the vertical direction was known to be almost the same as in the horizontal direction as seen in a view of a luminescence plate that was temporarily inserted during the beam tuning.

Three tracking devices—the vertex tracking chamber (VTC), cylindrical drift chamber (CDC), and barrel drift chamber (BDC)—were used to determine the trajectories of the charged particles. In the present analysis the momentum was determined by using CDC and BDC. The momentum resolution σ_p was $\sigma_p = \sqrt{(1.37\% \cdot p)^2 + 0.41\%^2} \cdot p$ (GeV/c), where p is the momentum of a particle.

For electron identification, two types of gas Čerenkov counter (FGC and RGC) and three types of lead glass calorimeter (SLG, RLG, and FLG) were employed. The gas Čerenkov counters were horizontally segmented into 6°. The radiator of the gas Čerenkov counters was isobutane at room temperature and atmospheric pressure. The refractive index is 1.00127 at standard temperature and pressure, which corresponds to a momentum threshold of 2.26 GeV/c for charged pions. All lead glass detectors were built with SF6W [24] and were typically segmented to 3.5° horizontally. The typical energy resolution for 1 GeV electrons is 0.15 GeV. The acceptance for electrons ranged from $\pm 12°$ to $\pm 90°$ in the horizontal direction and from $-22°$ to $22°$ in the vertical direction.

The counters for kaon identification were start timing counters (STC), hodoscopes (HC), aerogel Čerenkov counters (AC), and time-of-flight counters (FTOF). The acceptance for kaons ranged from $\pm 12°$ to $\pm 54°$ in the horizontal direction and from $-6°$ to $6°$ in the vertical directions. The three counters (STC, AC, and FTOF) were horizontally segmented to 6°, and

TABLE I. Summary for the targets, beams, and trigger modes used in the present analyses. In the 2002 run, four Cu targets were used.

Year	Target	Position (mm)	Interaction length (%)	Radiation length (%)	Number of protons	Trigger
1999	CH_2	-48	0.111	0.195	3.0×10^{13}	electron/kaon
	C	38	0.106	0.213		
	Cu	-7	0.0391	0.412		
2002	C	0	0.213	0.431	3.2×10^{14}	electron
	Cu	$\pm24, \pm48$	4×0.0539	4×0.565		

HC was typically segmented horizontally to $3°$. The time of flight (TOF) of charged particles was measured by using STC and FTOF with a resolution of 0.36 ns and flight length of about 3.7 m. Kaons and pions were separated in a momentum range from 0.53 to 1.88 GeV/c by using an aerogel with a refractive index of 1.034.

The electron trigger signal required a hit in FGC accompanied by a geometrical coincidence with RGC, SLG, or RLG. To select events containing e^+e^- pairs with large opening angles, both the left and the right arms were required to contain at least one e^+ or e^- candidate. The typical efficiency of the trigger for the electron pairs in the acceptance was 92.4%.

The kaon trigger signal was obtained from the coincidence of STC, HC, and FTOF. The charged pion contamination was reduced by using AC as a veto trigger. Proton contamination was reduced by setting a TOF window for the kaons by using a rough momentum value calculated by combining the hits in STC, HC, and FTOF in the trigger.

The number of recorded events for electron data were 7.41×10^7 and 5.08×10^8 in 1999 and 2002, respectively. A detailed description of the spectrometer can be found in Ref. [25].

III. DATA ANALYSIS

A. Analysis of ω and $\phi \to e^+e^-$ in $p + $ C and $p + $ Cu collisions

1. Event reconstruction

The charged tracks were reconstructed from hit positions in the drift chambers by using the Runge-Kutta fitting method. After the tracks were reconstructed, tracks corresponding to momenta between 0.4 and 2.0 GeV/c were selected for further analyses. The lower limit in the momentum range was set based on the threshold of the trigger, whereas the upper was set in order to avoid pion contamination above the gas Čerenkov threshold.

Pairs of positive and negative tracks were necessary to satisfy the trigger condition. All the e^+ and e^- candidates were reexamined so that an FGC hit association could be obtained with an RGC, SLG, or RLG association, depending on the location of the track. For candidates associated with lead glass calorimeters, the momentum ratio E/p should be larger than 0.5 for energy in the calorimeters to be obtained. We chose the value of 0.5, balancing the purity of e^+ and e^- with the

statistics of the present data. Figure 3 shows the distribution of the energy and momentum of the present data with FGC associations. In this figure it is clearly seen that electrons range along the line of $E = p$. After an e^+e^- pair was detected, we simultaneously refitted the e^+ and e^- tracks by constraining them to have the same vertex point on the interaction target. Finally, we identified 5.69×10^5 e^+e^- pairs.[1]

The reconstruction efficiency of the tracks from the targets was evaluated by both an eye-scan and a detector simulation using GEANT4 [26].

In the former method, first we used only one of the two arms and determined the target in which an interaction occurred. Then we visually scanned about 200 event displays and found track candidates in the other arm by using the drift chamber hit information with help from the interaction point. The tracking efficiency was evaluated by seeing whether the tracking program could find those eye-scanned track candidates. The efficiency was found to be 67% on average.

In the detector simulation method, the reconstruction efficiency was evaluated by using simulation tracks embedded in the real data. According to this method, the efficiency was found to be 78%.

---

[1] In a further analysis, we used only events in which e^+ went into the left arm and e^- went into the right arm, because the number of events satisfying the opposite criterion composed only 6% of the data.
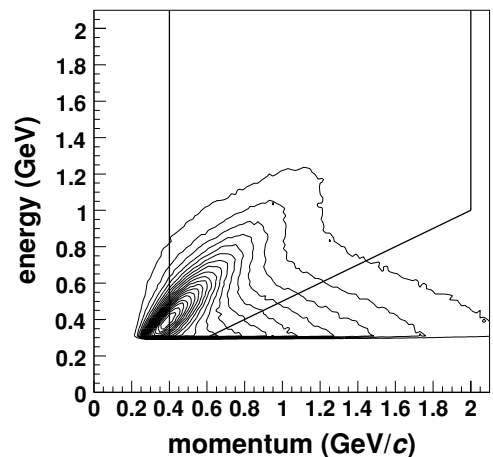

FIG. 3. Contour plot of the distribution of energy and momentum of the present data with FGC associations. The solid line shows the criterion of electron identification described in this article.

To combine the results of the two evaluations, we simply assumed the average 73% to be the efficiency in the present analysis and considered half the difference as a systematic error. The reason for this discrepancy is unknown, and this is one of the major sources of the systematic uncertainty in the present data analysis.

The inefficiency of the vertex reconstruction process was evaluated as follows. We took all the combinations of e^+ and e^- tracks regardless of the position of the closest point of each pair and obtained the yield of the ω meson peak. Then we used the vertex reconstruction program and required that event vertex belong to any of the target disks. In addition, we fit the e^+ and e^- tracks together by constraining them to have the same vertex point on the interaction target and required that the χ^2 over the number of degrees of freedom (NDF) should be less than 5. As a result, we lost 6.0% of the ω meson yield, so that the vertex reconstruction efficiency was 94.0%.

Contaminations due to the misidentification of pions and other particles in the present data were evaluated at the mass region of the ω meson, i.e., from 0.75 to 0.80 GeV/c^2, by tightening the electron identifications with gas Čerenkov counters and lead glass calorimeters until the misidentification becomes negligibly small. In this mass region, in the $p + $ C data, we found that 18% of the events result from misidentification and 18% are from uncorrelated e^+e^- pairs.

2. Corrections

Besides the tracking efficiency, several detector effects were evaluated and corrected as described below. The efficiencies of the electron identification counters were evaluated as a function of momentum by using pure electron samples from γ conversions and Dalitz decays. These electron samples were identified as a zero-mass peak in the e^+e^- spectra, and they were not required to participate in the trigger to avoid trigger bias. The obtained efficiencies were typically 85% for FGC, 86% for RGC, and 97% for the lead glass counters.

The energy losses of the tracks through the detectors were estimated by using GEANT4 simulation. Typically, the reconstructed momentum gave a lower value by 3 MeV/c for a 1 GeV/c electron owing to the energy loss. The momentum difference was corrected track by track by using a correction table obtained by the simulation. It should be noted that this correction compensated only mean energy loss. For effects that cause an eventual large energy loss like bremsstrahlung, the corrections were carried out in a different manner, as described later.

The geometrical acceptances for vector mesons V were obtained as functions of the invariant mass, rapidity y, and transverse momentum p_T by the simulation. The acceptances were averaged over azimuth φ, and isotropic decays of $V \to e^+e^-$ were assumed. The effects of the trigger, i.e., requirements of a geometrical correlation between the electron identification counters, were also considered. In order to obtain the yields of vector mesons, mass spectra were corrected for the acceptance in the mass range above 0.55 GeV/c^2. Below 0.55 GeV/c^2, the correction was too large to evaluate reliable values. The obtained acceptances at the ω and the ϕ meson masses are tabulated in Fig. 4.
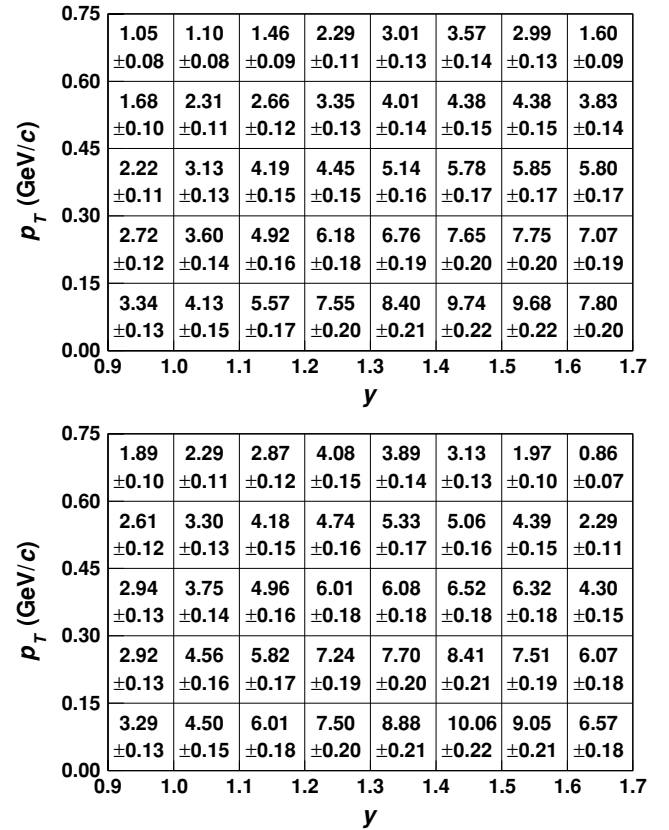

FIG. 4. Acceptances (%) for ω meson mass (top) and ϕ meson mass (bottom) as functions of y and p_T of the mesons. The errors are statistical and are obtained from the simulation.

3. Spectrum decomposition

In Fig. 5, the top and the bottom pairs of panels show the spectra of the invariant mass of e^+e^- pairs in the range of $0.9 < y < 1.7$ and $p_T < 0.75$ GeV/c without and with the acceptance correction, respectively. The peaks of ω and ϕ are distinctly observed.

The e^+e^- mass spectra were fitted and decomposed into the dielectron decays $\omega \to e^+e^-$, $\phi \to e^+e^-$, and $\rho^0 \to e^+e^-$; the Dalitz decays $\eta \to \gamma e^+e^-$, $\omega \to \pi^0 e^+e^-$, $\phi \to \pi^0 e^+e^-$, and $\phi \to \eta e^+e^-$; and the combinatorial background. The origins of the combinatorial background were pairs that were picked up from two independent Dalitz decays or γ conversions, and pairs like $e^\pm \pi^\mp$ that were due to misidentification. The Dalitz decay $\pi^0 \to \gamma e^+e^-$ contribution is negligible in the acceptance of the present data.

For the invariant mass distributions of the $\omega \to e^+e^-$ and $\phi \to e^+e^-$ decays, we used in the fit a Breit-Wigner function

$$\frac{d\sigma}{dm} = \frac{N}{(m - m_0)^2 + \Gamma_{\text{tot}}^2/4} \tag{2}$$

convoluted with a Gaussian function for the experimental resolution. If the relativistic Breit-Wigner shape is used instead, the results do not change significantly. Here σ is the cross section; m, the invariant mass of the e^+e^- pair; N, a normalization factor; m_0, the meson mass; and Γ_{tot}, the natural decay width. For the shape of the $\rho^0 \to e^+e^-$
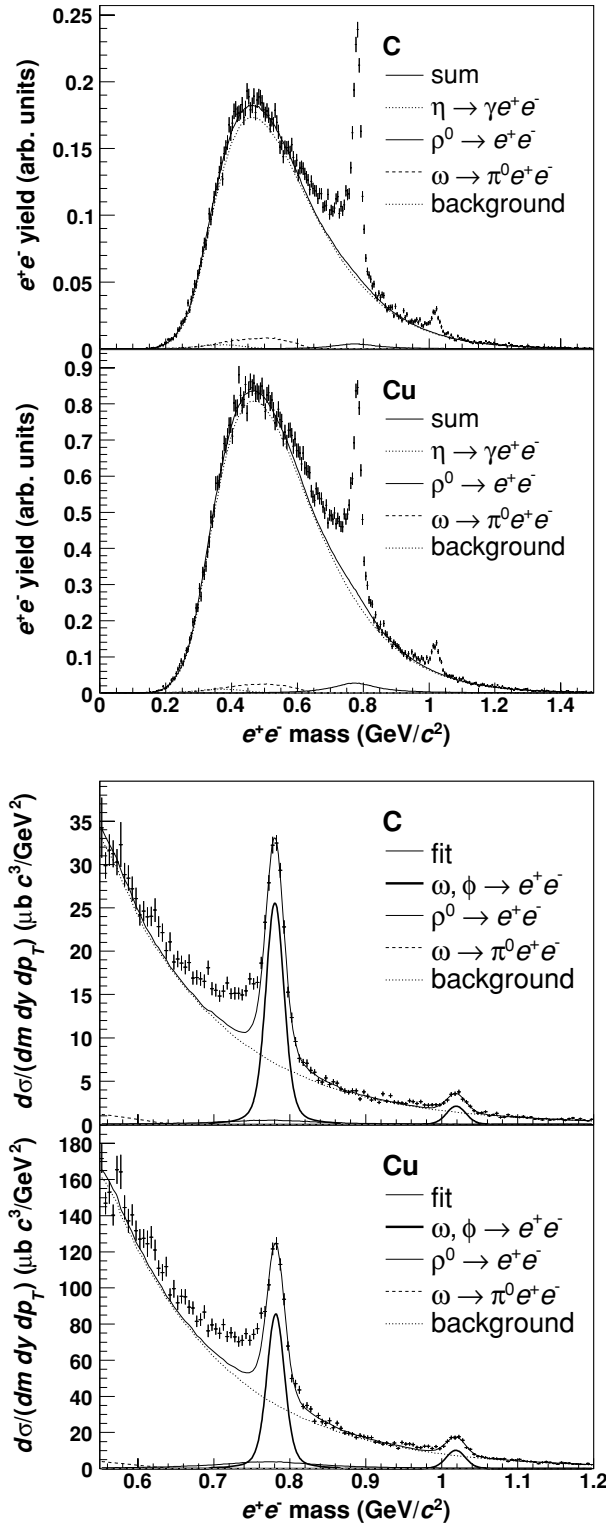
FIG. 5. The e^+e^- mass distributions of the acceptance-uncorrected data (top panels) and the corrected data (bottom panels) in the kinematic range of $0.9 < y < 1.7$ and $p_T < 0.75$ GeV/c. The curves in the top panels represent the backgrounds, Dalitz components, ρ^0 components, and their sum. The amount of e^+e^- decays of ω and ϕ mesons is represented by thick solid curves in the bottom panels, and the thin solid curves represent the sum of all the components. The number of ϕ meson Dalitz decays is negligibly small.

decay, we used the relativistic Breit-Wigner shape

$$\frac{d\sigma}{dm} = \frac{N}{\left(m^2 - m_{\rho^0}^2\right)^2 + m^2\Gamma_{\text{tot}}^2} \qquad (3)$$

instead of the Breit-Wigner function. To obtain the mass distribution in the spectrometer acceptance, we used the GEANT4 simulation with an input momentum distribution of ρ^0 mesons that was obtained using JAM. The e^+e^- invariant mass spectra from the Dalitz decays of η, ω, and ϕ mesons were also obtained by the simulation. Their e^+e^- distributions were determined by following the vector meson dominance model given in Ref. [27] by using the mother meson distributions obtained by JAM. The combinatorial background shape was evaluated by using an event mixing method, combining e^+ and e^- tracks picked from different events.

The free parameters of the fit were the yields, the peak positions, and the mass resolutions of ω and ϕ mesons; the yields of η and ρ^0 mesons; and the number of the background events. As mentioned above, the spectra were corrected in a mass range only above 0.55 GeV/c^2. Therefore, below 0.55 GeV/c^2, the uncorrected spectra were used in the fit mainly to accurately obtain the amount of the background. Although the fit region was from 0.20 to 1.2 GeV/c^2, the mass regions from 0.600 to 0.765 GeV/c^2 and from 0.955 to 0.985 GeV/c^2 were excluded to avoid the effect of the excesses below the ω and ϕ peaks, which in other publications [5–7] we have claimed as the signal of the mass modification. In the present analysis, however, we did not assume any underlying physics for the excess, and we aimed only to obtain the yields of ω and ϕ mesons correctly, as discussed below.

The fit results are shown by thin solid curves in Fig. 5. The χ^2/NDF were obtained as 157/152 and 192/152 for the $p + \text{C}$ and $p + \text{Cu}$ interactions, respectively.

After obtaining the raw yields of the ω and ϕ mesons by the fit, the correction for hard energy losses such as bremsstrahlung or a radiative tail was applied. The hard energy loss causes a low mass tail in the invariant mass distribution. The loss of the yield due to this tail could not be evaluated by the procedure described above; hence, we performed studies using the GEANT4 simulation. The yields of the tails with respect to the integrals of the Breit-Wigner peaks were found to be $11.9 \pm 1.0\%$ for the ω mesons and $10.4 \pm 0.8\%$ for the ϕ mesons. These values were simply added to the peak yields. The uncertainty of these corrections includes an ambiguity with respect to the cross sections of such hard energy losses in GEANT4.

By the fit procedure described above, the peak position and mass resolution of the ϕ meson were obtained as 1019 ± 1 and 11.8 ± 1.0 MeV/c^2, respectively. The peak position of the ϕ meson is consistent with the values of the Particle Data Group [28], and the mass resolution is consistent with the simulation value of 10.7 MeV/c^2; however, the peak position of the ω meson was found to be lower by 2.2 MeV/c^2. The width of the omega mesons was also broader than that expected by the simulation.[2] Here we adopted a conservative approach

———————

[2]If we take internal bremsstrahlung into account, the peak positions of both the ω mesons and the ϕ mesons agree with the expected positions.

to obtain the yield of unmodified ω mesons by estimating the additional systematic error due to this peak shift. The error for the ω meson yield was evaluated as 0.48% for a $p + C$ interaction and 1.8% for a $p + Cu$ interaction, which were obtained by forcing the peak position in the fit to the higher value of 2.2 MeV/c^2. The momentum scale and resolution were also verified by using the $K_s \rightarrow \pi^+\pi^-$ data [7]. The measured peak position of K_s was 496.8 ± 0.3 MeV/c^2, which was consistent with that of the simulation result, 496.9 MeV/c^2. The measured mass resolution of K_s was 3.9 ± 0.4 MeV/c^2, which was expected to be 3.5 MeV/c^2 by the simulation.

4. Systematic errors

In addition to the uncertainties described previously, the following systematic uncertainties were studied to obtain the cross sections.

The uncertainty in the background shapes could be a source of the systematic error. The background was a result of uncorrelated pairs that were obtained from two independent Dalitz decays, γ conversions, or other meson decays. The background shape was obtained by an event mixing technique. In the mixing process, it is possible that the correlated e^+e^- pairs from the decays of ρ^0, ω, and ϕ mesons deform the estimated background shape; this could result in a systematic error. In order to estimate the systematic error, two methods were used in the event mixing. One was to use all electrons except for those belonging to the ω and ϕ meson mass regions, which are 0.765 to 0.800 GeV/c^2 and 0.995 to 1.035 GeV/c^2, respectively. In the other method we used all the pairs in the event mixing but with weights in order to obtain a self-consistent shape of the background. The weights were obtained as a function of the e^+e^- mass as the ratio of the background shape to the real mass spectrum, and they were self-consistently determined by repeating the fit several times. We adopted the latter method to determine the background shape. The difference between the two methods was assigned as a systematic error. The difference in the yield of ω mesons was 0.23% and that in ϕ mesons was 0.60%.

The normalization and spectral shape of the combinatorial background were affected by all the other correlated e^+e^- components, since they were obtained by the fit. The systematic errors in the peak-yield determination due to the ambiguity of the Dalitz decays of η, ω, and ϕ mesons were evaluated by doubling or eliminating those yields and refitting the mass spectra. These systematic errors were found to be 0.62% and 0.85% for ω and ϕ mesons, respectively.

It was difficult to consider the uncertainty of the ρ^0 shape, since the mass region from 0.600 to 0.765 GeV/c^2 could not be represented by known sources, and the shape of the mass modification was not well understood. In this analysis we simply considered the relativistic Breit-Wigner shape for the ρ^0 distribution and performed a fit by excluding the excess region. In order to evaluate the systematic error, we fixed the ρ^0 yield at zero as an extreme case and reperformed the fit. In this fit, the ω yield increased by 3.19% for the carbon target and 7.65% for the copper target; further, the ϕ meson yield

TABLE II. Systematic uncertainties for ω and ϕ meson yields for the data taken in 2002.

Data	ω (%)	ϕ (%)
Beam intensity	10	10
C target thickness	0.28	0.28
Cu target thickness	0.55	0.55
Trigger electronics	3.8	3.8
Track reconstruction	14.9	14.9
Vertex reconstruction	4.7	4.7
Acceptance	1.23	1.25
Hard energy loss	1.18	0.94
Electron identification	2.92	2.60
Background shape	0.23	0.60
Mass scale for $p + C$	0.48	
Mass scale for $p + Cu$	1.83	
Dalitz yield	0.62	0.85
ρ^0 from $p + C$	3.2	3.5
ρ^0 from $p + Cu$	7.6	5.5
Total for $p + C$	19.5	19.5
Total for $p + Cu$	20.8	20.0

increased by 3.45% and 5.48% for each of the above targets, respectively. We considered these values as systematic errors due to the unknown ρ^0 distribution. It should be noted that the ω mesons can also be modified such that the ω cross sections obtained in the present analysis are only for that component whose shape is consistent with the unmodified shape.

A possible cause of another error might lie in the efficiency estimations for electron identification. These uncertainties were evaluated by using the error bands of efficiency curves of electron identification counters and were obtained as 2.92% for ω mesons and 2.60% for ϕ mesons.

All the systematic errors are summarized in Table II. In the evaluation of the absolute cross section, the errors of the beam intensity, target thicknesses, and efficiency of the trigger electronics were also considered. In summary, the systematic errors for the cross sections for ω mesons were 19.5% for the carbon target and 20.8% for the copper target, and those of ϕ mesons were 19.5% and 20.0%, respectively.

The systematic errors for the α parameters are due only to the items that differ between carbon and copper targets. These are listed in Table III. In summary, the uncertainties for the α parameters of ω and ϕ mesons were 5.2% and 1.9%, respectively.

B. Extraction of the cross section in $p + p$ interaction

The target subtraction method was employed to obtain the cross section in $p + p$ collisions; this was achieved by using the data taken in 1999. The production cross sections $\sigma(p)$ in $p + p$ collisions were calculated by the formula $\sigma(p) = [\sigma(CH_2) - \sigma(C)]/2$ in the region of $0.9 < y < 1.7$ and $p_T < 0.6$ GeV/c. The analysis was performed in almost the same manner as that for the data in 2002.

TABLE III. Systematic uncertainties for α parameters of ω and ϕ mesons for the data taken in 2002.

Data	ω (%)	ϕ (%)
Acceptance	1.47	1.13
Target thickness	0.52	0.39
Background shape	0.27	0.54
Mass scale	1.13	
Dalitz yield	0.37	0.48
ρ^0 yield	4.89	1.25
Total	5.2	1.9

To minimize the uncertainty due to experimental differences between the 1999 and 2002 data, we normalized the yield of ω mesons with carbon targets in the 1999 data to that in 2002 data and extracted the absolute cross sections in $p + p$ collisions. Another uncertainty arose from the difference in the target thicknesses that were measured with an accuracy of 0.8%. We obtained 20.1% and 20.0% as the systematic uncertainty in $p + p$ collisions for the ω meson production and ϕ meson production, respectively.

IV. RESULT AND DISCUSSION

A. Global feature of the obtained results

From the decay branching fractions listed in Table IV, the differential cross sections of the inclusive ω meson production are obtained as $14.30 \pm 0.34(\text{stat}) \pm 2.79(\text{syst})$ mb·c/GeV and $46.63 \pm 1.25(\text{stat}) \pm 9.70(\text{syst})$ mb·c/GeV in $p + \text{C}$ and $p + \text{Cu}$ collisions in the region of $0.9 < y < 1.7$ and $p_T < 0.75$ GeV/c, respectively; further, those of ϕ meson production are $0.270 \pm 0.017(\text{stat}) \pm 0.053(\text{syst})$ mb·c/GeV and $1.290 \pm 0.070(\text{stat}) \pm 0.258(\text{syst})$ mb·c/GeV, respectively.[3] The α parameters of ω and ϕ mesons are obtained as $0.710 \pm 0.021(\text{stat}) \pm 0.037(\text{syst})$ and $0.937 \pm 0.049(\text{stat}) \pm 0.018(\text{syst})$, respectively. The difference is $0.227 \pm 0.054(\text{stat}) \pm 0.041(\text{syst})$, and it is statistically significant.

In order to compare the production cross sections in the e^+e^- decay channels with those in the K^+K^- decay channel and the previous measurement of 12 GeV/c $p + p \rightarrow \rho^0 X$ by Blobel *et al.* [29], the present data were extrapolated to the backward hemisphere—the region $x_F < 0$ or $y < 1.66$, where

---

[3]In this article, neither the effect of internal bremsstrahlung nor the uncertainty of the branching fractions is considered.

TABLE IV. Branching fractions in the tables of the Particle Data Group [28].

Decay mode	Branching fraction
$\omega \rightarrow e^+e^-$	$(6.96 \pm 0.15) \times 10^{-5}$
$\phi \rightarrow e^+e^-$	$(2.96 \pm 0.04) \times 10^{-4}$
$\phi \rightarrow K^+K^-$	$49.2^{+0.6}_{-0.7}\%$

TABLE V. Meson production cross section in the backward hemisphere. The first errors are statistic, where as the second errors are systematic. The data points are plotted in Fig. 6.

Collision	ω (mb)	ϕ (e^+e^-) (mb)	ϕ (K^+K^-) (mb)
H	$2.3\pm1.1\pm0.5$	$0.034\pm0.045\pm0.007$	$0.03\pm0.19\pm0.01$
C	$13.4\pm0.3\pm2.6$	$0.240\pm0.015\pm0.047$	$0.39\pm0.05\pm0.19$
Cu	$49.0\pm1.3\pm10.2$	$1.21\ \pm0.07\ \pm0.24$	$1.84\pm0.27\pm0.89$
Pb			$6.0\ \pm1.8\ \pm2.9$

x_F is Feynman's x. The production cross sections in the backward hemisphere are listed in Table V. The correction factors for this extrapolation from the measured regions—$0.9 < y < 1.7$ and $p_T < 0.75$ GeV/c—to the backward hemisphere were calculated by using JAM, since the shapes of p_T and y spectra are consistent with the result of JAM calculation, as described below.

The cross sections of the inclusive ϕ meson production in the K^+K^- decay channel are also listed in Table V. These were obtained from the previous analysis in this experiment [30,31]. The α parameter of the ϕ meson production measured in the K^+K^- decay channel is obtained as 1.01 ± 0.09 by using the $p + p$, $p + \text{C}$, $p + \text{Cu}$, and $p + \text{Pb}$ data in the spectrometer acceptance; this value is statistically consistent with the present e^+e^- analysis.

Figure 6 shows the cross sections in the backward hemisphere as a function of the nuclear mass number. The dotted curves represent the result of the JAM calculation, and the solid and dashed lines represent the measured α
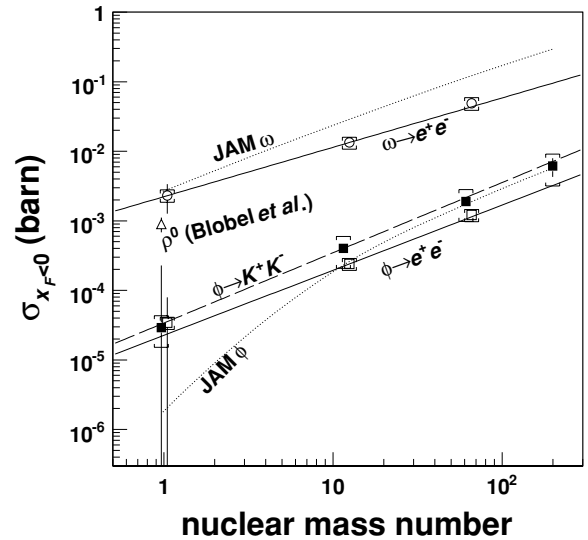

FIG. 6. Production cross section in the backward hemisphere as a function of mass number. The circles, open squares, and filled squares show the cross section of ω mesons, ϕ mesons measured in the e^+e^- decay channel, and those in the K^+K^- decay channel, respectively. The vertical lines represent the statistical errors, and the brackets represent the systematic errors. The previous $p + p \rightarrow \rho^0 X$ measurement [29] is indicated by a triangle. The dotted curves represent the prediction by JAM simulation results. The solid and dashed lines represent the α parametrization (see text).
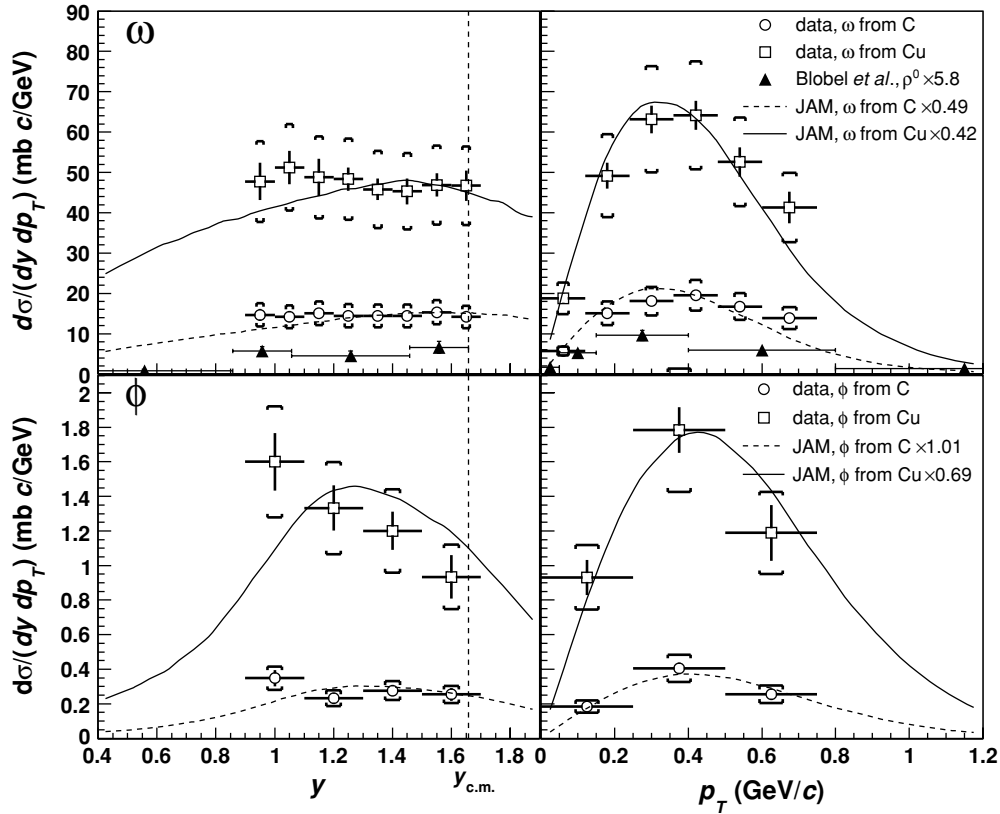
FIG. 7. Differential cross sections of ω (top) and ϕ (bottom) mesons as functions of y (left) or p_T (right). The statistical errors are represented by vertical bars, and the systematic errors are represented by brackets. The previous $p + p \rightarrow \rho^0 X$ measurement [29] is indicated by triangles after being scaled up with the nuclear mass number dependence obtained in the present analysis. The dashed and solid curves represent scaled cross sections of JAM in $p + C$ and $p + Cu$ collisions, respectively. The rapidity of the center of mass system is 1.66, as indicated by $y_{c.m.}$. The data points are listed in Table VI.

parametrization. The α parameters shown in the figure were 0.710, 0.937, and 1.01 for the data of $\omega \rightarrow e^+e^-$, $\phi \rightarrow e^+e^-$, and $\phi \rightarrow K^+K^-$, respectively. It should be noted that these values were obtained from the data within the spectrometer acceptance before they were extrapolated to the backward hemisphere.

The previous measurement [29] yielded the total cross section of 1.8 ± 0.25 mb for ρ^0 mesons. By assuming a ρ^0/ω ratio of 1.0 ± 0.2,[4] we obtain the ω meson production in the backward hemisphere as 0.90 ± 0.22 mb for a comparison with the present measurement. The triangle in Fig. 6 represents the obtained value. The measured ω meson production cross section in the present $p + p$ collision data is consistent with the ρ^0 cross section of Ref. [6] within the error.

B. Differential cross section of ω and ϕ production measured in e^+e^- decays

In a region $0.9 < y < 1.7$ and $p_T < 0.75$ GeV/c, the differential cross sections of ω and ϕ mesons were obtained

for each y or p_T bin, as shown in Fig. 7. These are also listed in Table VI.

The previous $p + p \rightarrow \rho^0 X$ measurement [29] was plotted as triangles, as shown in Fig. 7. It should be noted that the data points were scaled by factors of 5.81 ($= 12^{0.71}$) for clarity.

The distributions obtained by the JAM calculation are compared with the measurements in Fig. 7. The total cross sections obtained from the JAM calculation are larger than that obtained from the data. Hence they are scaled by the factors 0.489 for $p + C \rightarrow \omega X$, 0.421 for $p + Cu \rightarrow \omega X$, 1.006 for $p + C \rightarrow \phi X$, and 0.686 for $p + Cu \rightarrow \phi X$. These scale factors were determined as the ratio of the total cross sections in the acceptance between the data and JAM. The shapes of the differential cross sections of JAM are consistent with the present data, although the absolute cross sections are systematically larger than the data.

Figure 8 shows the α parameters of ω and ϕ mesons obtained in the region of $0.9 < y < 1.7$ and $p_T < 0.75$ GeV/c. These are also listed in Table VI. The flat lines represent the averaged α parameters with the errors shown in the left column. The dotted and dashed curves represent the results of JAM for $p + C$ and $p + Cu$ collisions. Although the α parameters of the JAM calculation are significantly larger than those of the data, the difference between ω and ϕ mesons

---

[4]The ρ^0/ω ratio was measured by the reactions of $p + p \rightarrow \rho^0 +$ charged particles and $p + p \rightarrow \omega +$ charged particles [29].

TABLE VI. Differential production cross sections in $0.9 < y < 1.7$ and $p_T < 0.75$ GeV/c measured via e^+e^- decay channel. The first errors are statistical and the second are systematic. The data points are plotted in Figs. 7 and 8.

		ω from C (mb c/GeV)	ω from Cu (mb c/GeV)	α
y	0.9−1.0	14.7±1.5±2.9	47.8±4.6±10.0	0.708±0.083±0.042
	1.0−1.1	14.2±1.2±2.8	51.2±4.2±10.7	0.770±0.070±0.041
	1.1−1.2	15.0±1.1±3.0	48.8±4.6±10.2	0.706±0.071±0.040
	1.2−1.3	14.5±0.8±2.8	48.3±2.9±10.1	0.724±0.049±0.039
	1.3−1.4	14.4±0.8±2.8	45.8±2.7±9.6	0.693±0.048±0.039
	1.4−1.5	14.4±0.7±2.8	45.3±3.2±9.5	0.689±0.052±0.039
	1.5−1.6	15.3±0.7±3.0	46.9±2.9±9.8	0.671±0.045±0.038
	1.6−1.7	14.2±0.7±2.8	46.7±3.8±9.7	0.716±0.056±0.039
p_T (GeV/c)	0.00−0.12	5.7±0.4±1.1	18.8±1.2±3.9	0.714±0.057±0.038
	0.12−0.24	15.1±0.7±3.0	49.2±3.2±10.2	0.709±0.047±0.038
	0.24−0.36	18.1±0.8±3.5	63.1±3.4±13.2	0.750±0.042±0.039
	0.36−0.48	19.5±0.9±3.8	64.2±3.6±13.4	0.714±0.044±0.038
	0.48−0.60	16.8±1.3±3.3	52.6±3.6±11.0	0.687±0.063±0.040
	0.60−0.75	13.9±1.1±2.7	41.3±3.9±8.6	0.655±0.075±0.041
$0.9 < y < 1.7$, $p_T < 0.75$ GeV/c		14.30±0.34±2.79	46.63±1.25±9.70	0.710±0.021±0.037
		ϕ from C	ϕ from Cu	α
y	0.9−1.1	0.348±0.046±0.068	1.60±0.17±0.32	0.916±0.101±0.022
	1.1−1.3	0.232±0.032±0.045	1.33±0.13±0.27	1.050±0.101±0.020
	1.3−1.5	0.277±0.029±0.054	1.20±0.11±0.24	0.881±0.084±0.020
	1.5−1.7	0.255±0.037±0.050	0.93±0.13±0.19	0.780±0.119±0.019
p_T (GeV/c)	0.00−0.25	0.185±0.024±0.036	0.93±0.10±0.19	0.971±0.101±0.019
	0.25−0.50	0.405±0.032±0.079	1.78±0.13±0.36	0.890±0.066±0.019
	0.50−0.75	0.255±0.032±0.050	1.19±0.16±0.24	0.924±0.111±0.021
$0.9 < y < 1.7$, $p_T < 0.75$ GeV/c		0.270±0.017±0.053	1.290±0.070±0.258	0.937±0.049±0.018

in the α parameters is similar to what is seen in the JAM calculation.

C. Discussion

An interesting characteristic is the difference in the y dependence between ω and ϕ meson production cross sections. While the ω production is essentially independent of y, the ϕ production increases towards the smaller y values. In addition, the α parameters of ω and ϕ meson production are different by $0.227 \pm 0.054(\text{stat}) \pm 0.041(\text{syst})$. This significant difference in the α parameters confirms that the production mechanisms of ω and ϕ mesons are different.

One possible mechanism of ϕ meson production is a hard reaction between incident and projectile nucleons. If the hard reaction is dominant like J/ψ production at higher energies, α is expected to be around unity and independent of y. Further, the y distribution of the cross section is expected to be symmetric with respect to $y_{\text{c.m.}}$, which is not the case in the present ϕ production data.

Another possible explanation for the observed characteristics of the α parameter and cross sections is the effect of

secondary collisions in a target nucleus. In this case, no hard reaction is necessary. These effects are expected to increase in a smaller rapidity region for $p + A$ interaction, and the cross sections and α are expected to be larger in the backward region.

Although the JAM does not reproduce the data quantitatively, it yields fairly similar shapes in the inclusive cross sections of ω and ϕ meson productions; further, it also predicts the difference between the α parameters of these mesons. In the JAM calculation, more than 90% of the ϕ mesons are produced by secondary collisions mostly between nonstrange mesons and nucleons in a target nucleus, while ω mesons are produced both in primary and secondary reactions. For example, 30% and 50% of the ω mesons are produced in secondary reactions in the cases of 12 GeV $p + \text{C}$ and $p + \text{Cu}$ reactions in JAM, respectively. These differences in the production mechanism in JAM will surely be an important step to understand the measured differential cross sections.

The difference between the scaling factors applied to ϕ meson production in $p + \text{C}$ and $p + \text{Cu}$ collisions, in JAM, described in Sec. IV B, can be understood qualitatively by the overestimated contribution of the secondary collisions in
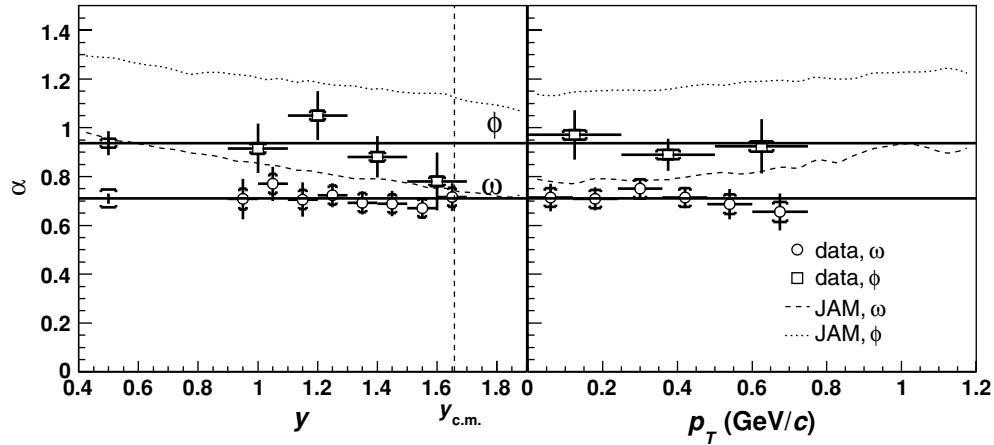
FIG. 8. The α parameters of ω (circle) and ϕ (square) mesons as functions of y (left) or p_T (right). The statistical errors are represented by vertical bars, and the systematic errors are represented by brackets. The horizontal lines represent the averaged α parameters of ω and ϕ mesons with the errors indicated on the left side. The dotted and dashed curves represent the α parameters of ϕ and ω mesons by JAM. The rapidity of the center of mass system is indicated by $y_{c.m.}$. The data points are listed in Table VI.

JAM. Although in those calculations almost all the ϕ mesons are produced in secondary collisions, the present data suggest that the contribution of the primary collisions can be larger. For the case of the ω meson, JAM just predicts larger absolute production yields than seen in the present data.

In summary, we measured the inclusive differential cross sections of the ω and ϕ meson production in $p + A$ collisions in the backward region. The difference in the α parameters between ω and ϕ mesons confirms that the production mechanisms of ω and ϕ mesons are different. The results are compared with the nuclear cascade calculations.

[1] G. Agakishiev *et al.*, Eur. Phys. J. C **4**, 231 (1998).

[2] G. M. Huber *et al.* (TAGX Collaboration), Phys. Rev. C **68**, 065202 (2003), arXiv:nucl-ex/0310011.

[3] K. Suzuki *et al.*, Phys. Rev. Lett. **92**, 072302 (2004), arXiv:nucl-ex/0211023.

[4] D. Trnka *et al.* (CBELSA/TAPS Collaboration), Phys. Rev. Lett. **94**, 192303 (2005), arXiv:nucl-ex/0504010.

[5] K. Ozawa *et al.* (E325 Collaboration), Phys. Rev. Lett. **86**, 5019 (2001), arXiv:nucl-ex/0011013.

[6] M. Naruki *et al.* (E325 Collaboration), Phys. Rev. Lett. **96**, 092301 (2006), arXiv:nucl-ex/0504016.

[7] R. Muto *et al.* (E325 Collaboration) (2005), arXiv:nucl-ex/0511019.

[8] M. Ono, J. Kishiro, S. Mikamo, A. Kusumegi, and T. Ishizuka, Phys. Lett. **B84**, 515 (1979).

[9] M. Binkley *et al.*, Phys. Rev. Lett. **37**, 571 (1976).

[10] B. Alessandro *et al.* (NA50 Collaboration), Eur. Phys. J. C **33**, 31 (2004).

[11] U. Husemann (HERA-B Collaboration), Nucl. Phys. B Proc. Suppl. **142**, 104 (2005), arXiv:hep-ex/0408110.

[12] A. N. Aleev *et al.* (BIS-2 Collaboration), Czech. J. Phys. **42**, 11 (1992).

[13] C. Daum *et al.* (ACCMOR Collaboration), Z. Phys. C **18**, 1 (1983).

[14] R. Bailey *et al.*, Z. Phys. C **22**, 125 (1984).

[15] B. B. Back *et al.* (E917 Collaboration), Phys. Rev. C **69**, 054901 (2004), arXiv:nucl-ex/0304017.

[16] Y. Akiba *et al.* (E-802 Collaboration), Phys. Rev. Lett. **76**, 2021 (1996).

[17] S. Okubo, Phys. Lett. **5**, 165 (1963).

[18] J. R. Ellis, M. Karliner, D. E. Kharzeev, and M. G. Sapozhnikov, Nucl. Phys. **A673**, 256 (2000), arXiv:hep-ph/9909235.

[19] S. von Rotz, M. P. Locher, and V. E. Markushin, Eur. Phys. J. A **7**, 261 (2000), arXiv:hep-ph/9912359.

[20] K. Nakayama, J. Haidenbauer, and J. Speth, Phys. Rev. C **63**, 015201 (2001), arXiv:nucl-th/0008047.

[21] Y. Nara, N. Otuka, A. Ohnishi, K. Niita, and S. Chiba, Phys. Rev. C **61**, 024901 (2000), arXiv:nucl-th/9904059, http://quark.phy.bnl.gov/ ynara/jam/.

[22] Y. Sugaya, Y. Yamanoi, J. Chiba, Y. Kiselev, M. Numajiri, H. Ochiishi, K. H. Tanaka, K. Yasuda, and Y. Yoshimura, Nucl. Instrum. Methods A **368**, 635 (1996).

[23] J. Simkin and C. W. Trowbridge, Rutherford Laboratory, RL-79-097 (1979), http://www.vectorfields.co.uk/.

[24] S. Kawabata, R. Sugahara, T. Tauchi, N. Ujiie, Y. Watanabe, S. Kuroda, and T. Suwada, Nucl. Instrum. Methods A **270**, 11 (1988).

[25] M. Sekimoto *et al.* (E325 Collaboration), Nucl. Instrum. Methods A **516**, 390 (2004).

[26] S. Agostinelli *et al.* (GEANT4 Collaboration), Nucl. Instrum. Methods A **506**, 250 (2003), http://wwwasd.web.cern.ch/wwwasd/geant4/geant4.html.

[27] A. Faessler, C. Fuchs, and M. I. Krivoruchenko, Phys. Rev. C **61**, 035206 (2000), arXiv:nucl-th/9904024.

[28] K. Hagiwara *et al.* (Particle Data Group), Phys. Rev. D **66**, 010001 (2002).

[29] V. Blobel *et al.* (Bonn-Hamburg-Munich Collaboration), Phys. Lett. **B48**, 73 (1974).

[30] S. Yokkaichi, Ph.D. thesis, Department of Physics, Faculty of Science, Kyoto University, 2000.

[31] M. Ishino, Ph.D. thesis, Department of Physics, Faculty of Science, Kyoto University, 2000.